2052-3

Summer College on Plasma Physics

10 - 28 August 2009

Spectroscopic Plasma Diagnostics

Ian Hutchinson
NSE, MIT
USA

Spectroscopic Plasma Diagnostics

I H Hutchinson

Plasma Science and Fusion Center

and Nuclear Science and Engineering Department

MIT, Cambridge, MA, USA

Overview of Spectroscopic Techniques

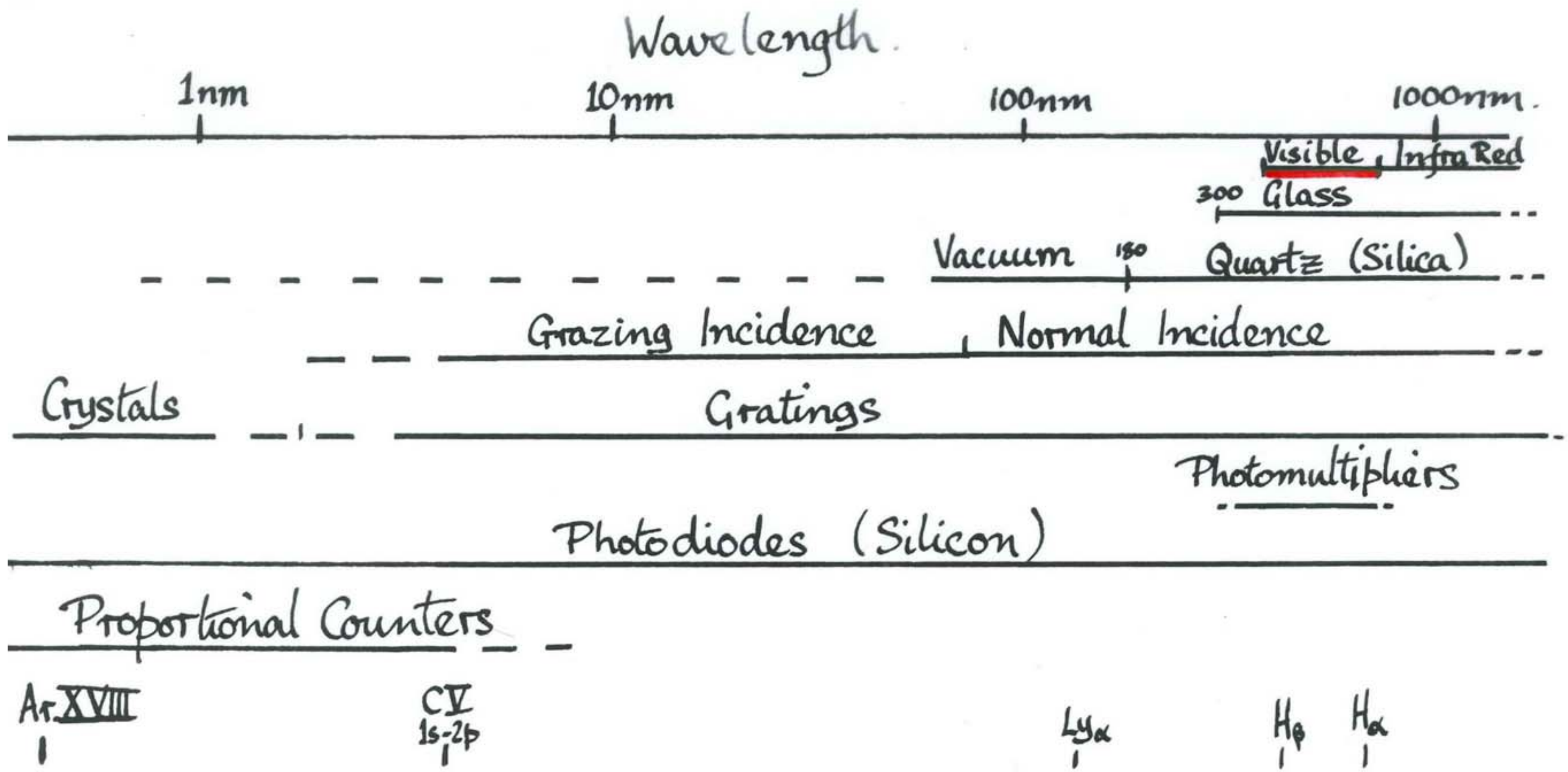

Technique depends on transmission of photons by materials; reflection properties; wavelength relative to mechanical or atomic spacing; photon energy relative to semi-conductor band gaps & ionization potential.

Line Radiation

$\hbar\omega = h\nu = E_i - E_j$ Photon energy.

$\lambda = 2\pi c/\omega = c/\nu$

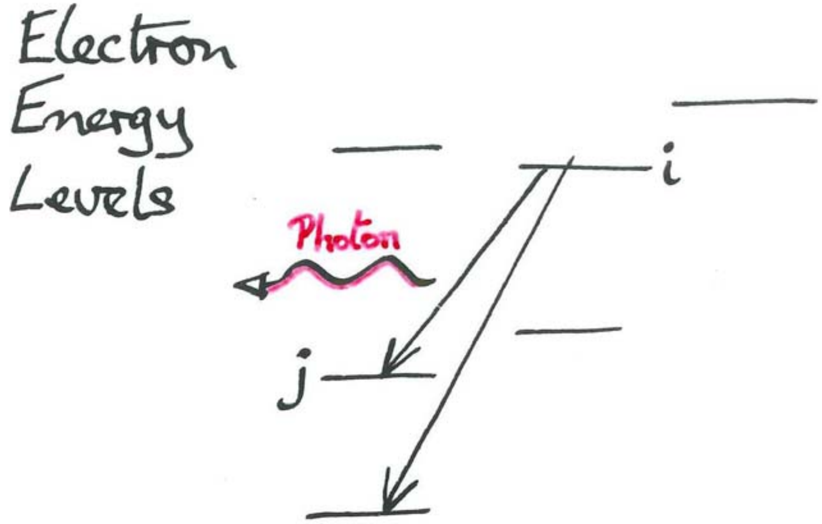

- Spontaneous transition probability (each i-atom): A_{ij} per unit time.
- Total number of transitions ($i \rightarrow j$) per unit volume per unit time:

$\boxed{A_{ij}.n_i}$ where n_i is density of i-atoms

Many different lines from each species

Many different species:

Neutral	+1	+2	+3	+4
OI	OII	OIII	OIV	...
CI	CII	CIII	CIV	...

Result: very complex spectra.

Example spectrograph

Rather old fashioned photographic plate.

Horizontal position corresponds to wavelength.

Relative intensity is important in line identification.

Rarely do we identify every single line.

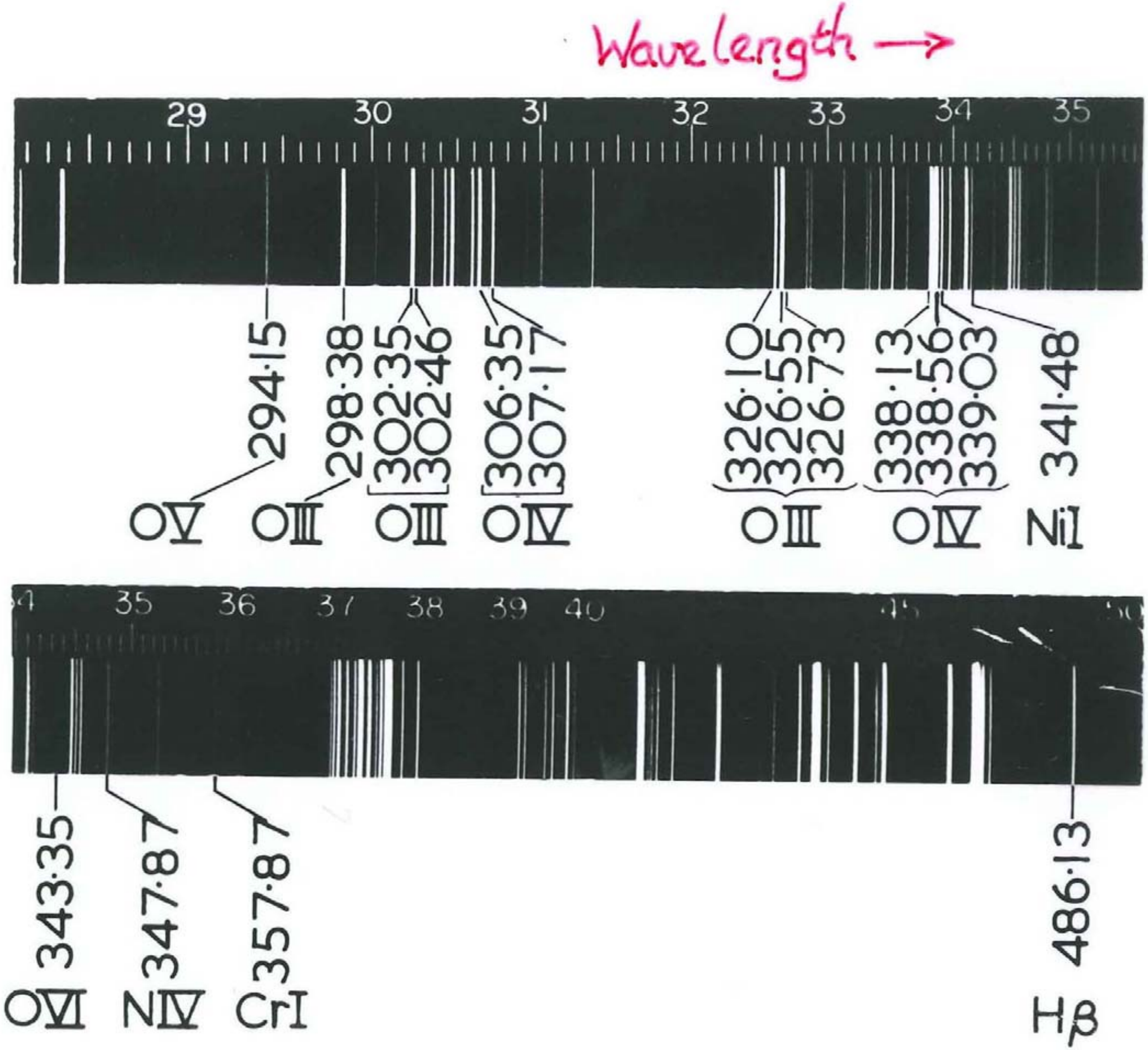

Defining View of Plasma

The view of plasma is defined by two apertures (and a spacing between them).
Each point in one aperture (A) collects from a solid angle Ω.

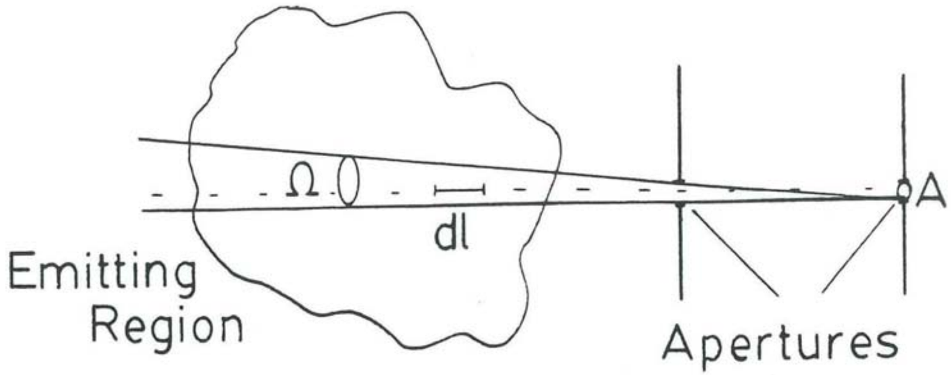

Number of photons detected (per unit time)

$$S = \underbrace{\eta}_{\text{Overall Efficiency}} \cdot \frac{\overset{\text{Area}}{A}\ \overset{\text{Solid Angle}}{\Omega}}{\underbrace{4\pi}_{4\pi\ \text{steradians}}} \int \underbrace{A_{ij}\ n_i}_{\text{Transitions /vol / time}}\ \underbrace{dl}_{\text{Length}}$$

- η includes losses in optical components detector efficiency, etc.
- $A\Omega$ is "étendue" $=$ light gathering power defined by optical collection system.

Assuming viewing path is narrow enough that $n_i \sim$ const across it (but not along beam).

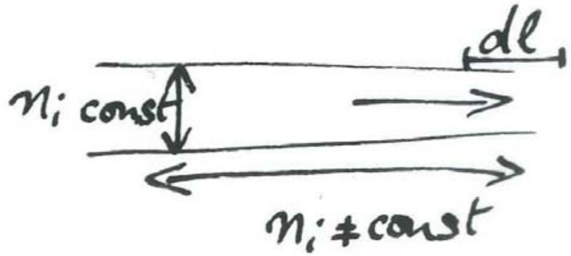

Measure (line average) density of excited state.

Deduce Species Density

Measure (impurity) **species density** by relating

Excited state n_i, which is the thing we actually observe,

to Ground state n_0 (or the total density of all states of this species).

Solving for the theoretical relationship between n_i and n_0 requires knowledge of

- Collisional Excitation rate $n_e < \sigma_{i'j'} v > (V_{i'j'}.)$
- Radiative rates $(A_{i'j'})$
- Sometimes other things (Recombination Charge Exchange)

Complicated solution of multi-parameter equations governing evolution of excitation state populations. (Keep theoretical spectroscopists employed.)

There are some simple cases (e.g. Thermal Equilibrium, Coronal Equilibrium). But these rarely apply to interesting plasmas.

More often complex, somewhat uncertain.

Spectrometers

Diffraction Grating Instrument: Typical Czerny-Turner.

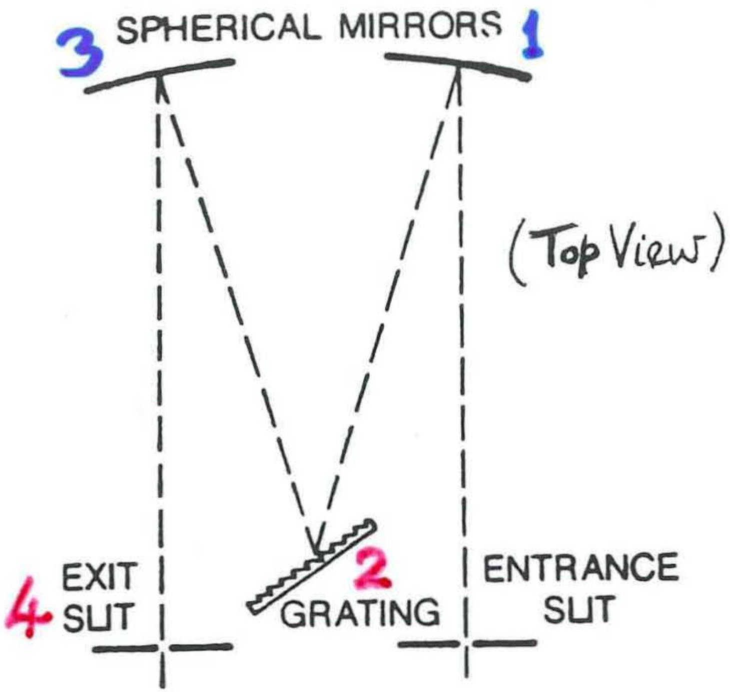

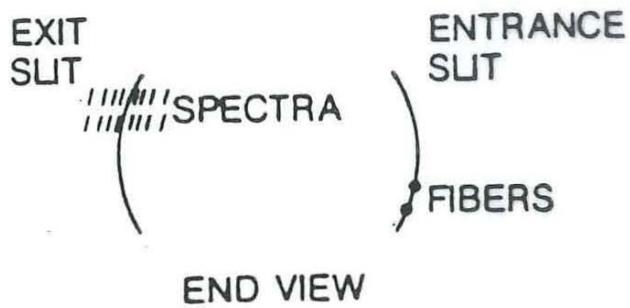

1. Spherical Mirror(s) → Plane Wavefront
2. Grating diffracts at angle dependent on wavelength (and grating angle).
3. Focussed to exit (4) slit. (Selects '1' wavelength).

Replace exit slit with detector array → Polychromator, spectrum.

Match input slit to different plasma positions → Multiple spectra.

Hirex

Dispersion of different λ

Imaging of different slit positions.

High Resolution Crystal X-ray Spectrometer.

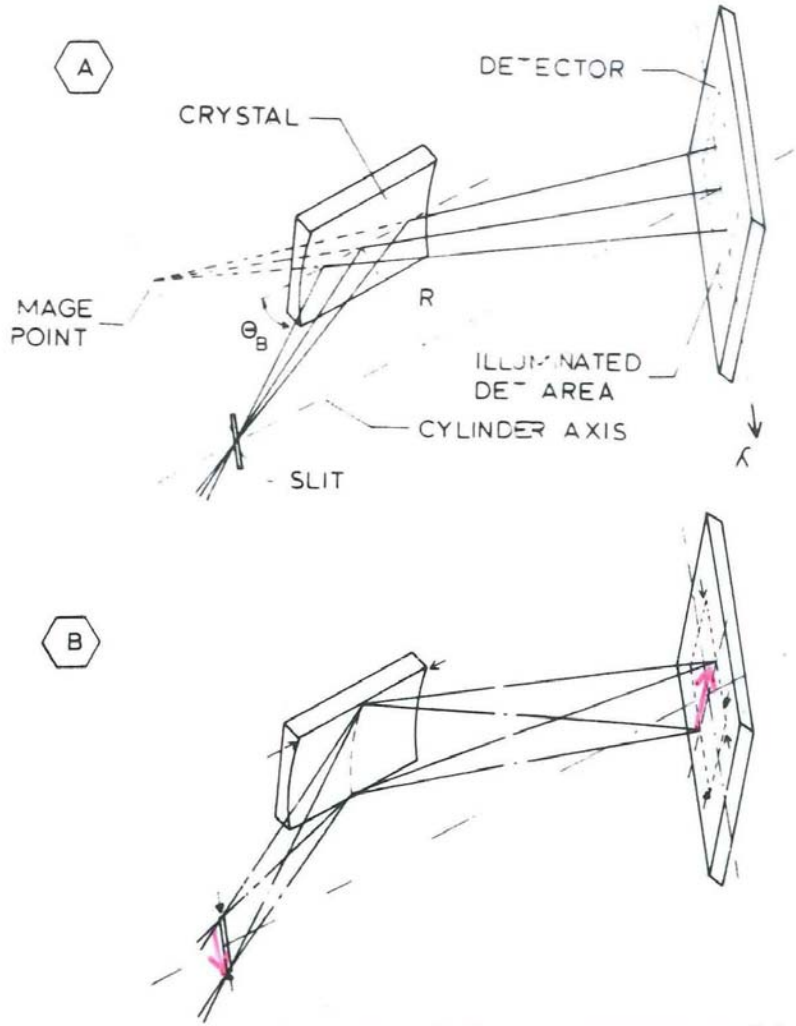

Fig. 1. Outline of the optics of the spectrometer used in the tokamak measurements. The wavelength dispersion is shown in A. and the vertical focusing and imaging in B. The entrance slit and the detector had Be windows to allow evacuation of the spectrometer; the slit was positioned close to a 5×15 mm^2 Be window on the tokamak.

TFTR Giant spectrometer 1990s

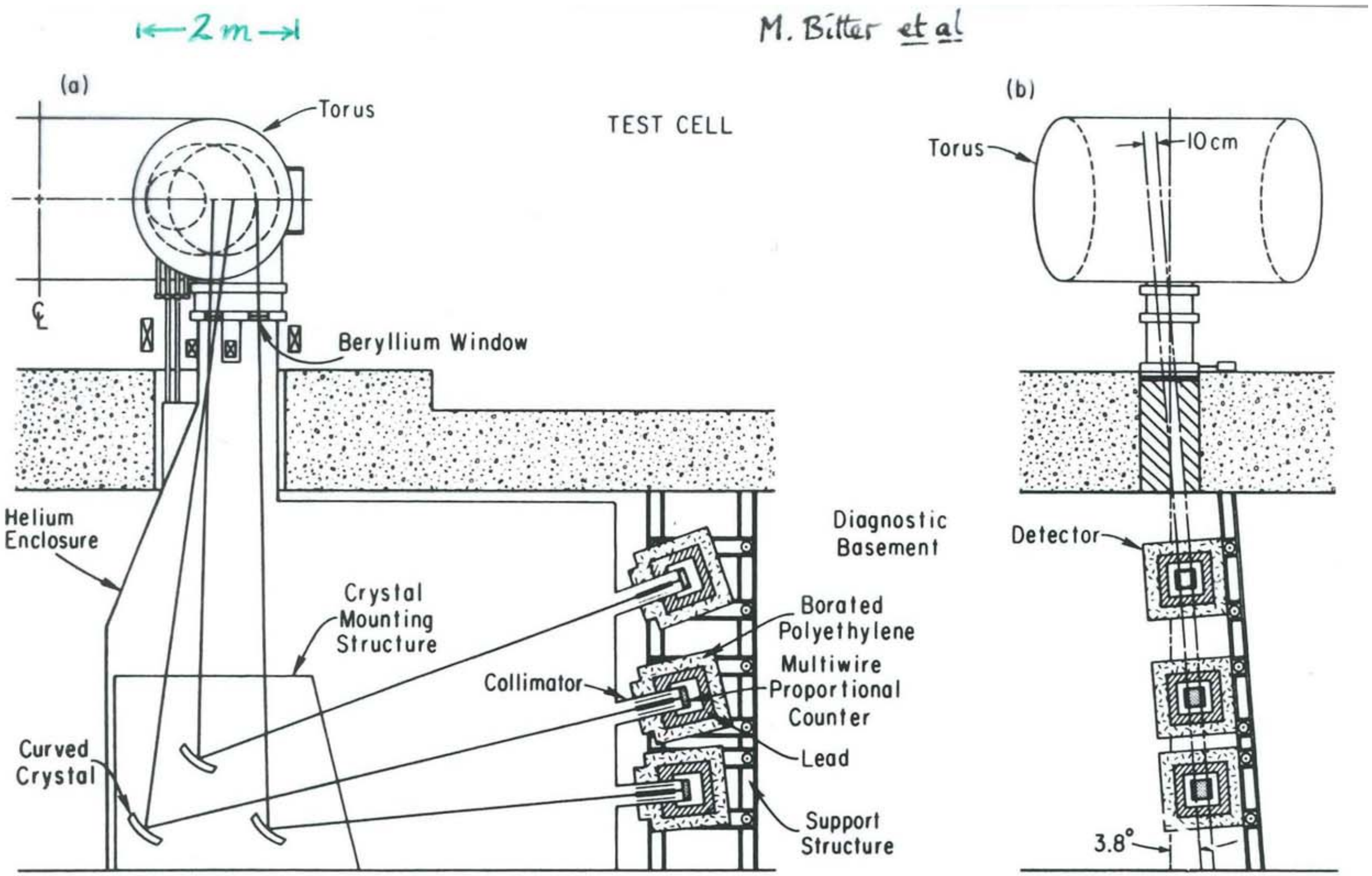

FIG. 1. Vertical Bragg x-ray spectrometer in the TFTR diagnostic basement.

Imaging Johann Spectrometer

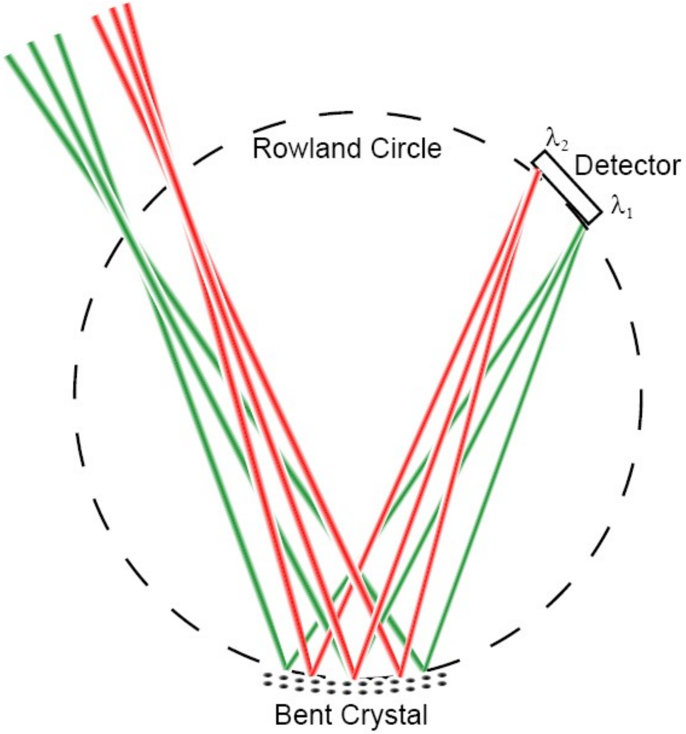

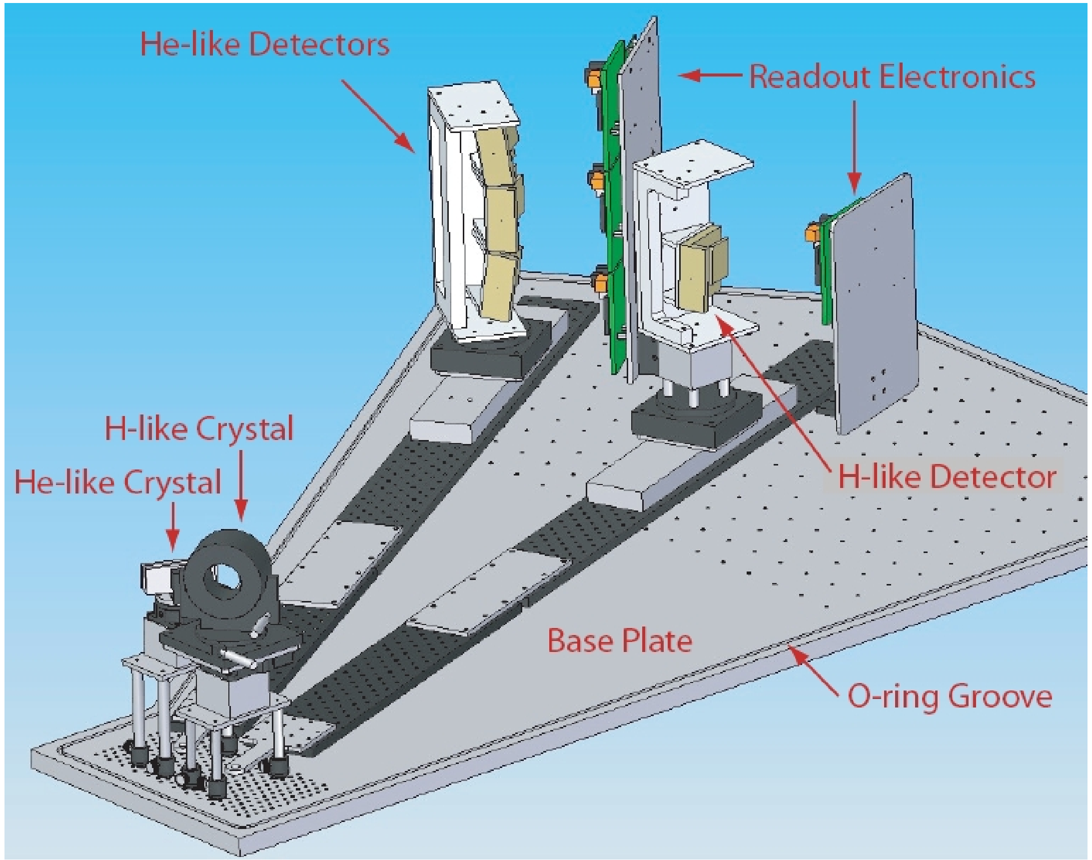

Spherically bent crystal

Needs no slits.

Enables simultaneous imaging of plasma and spectral resolution.

Top View

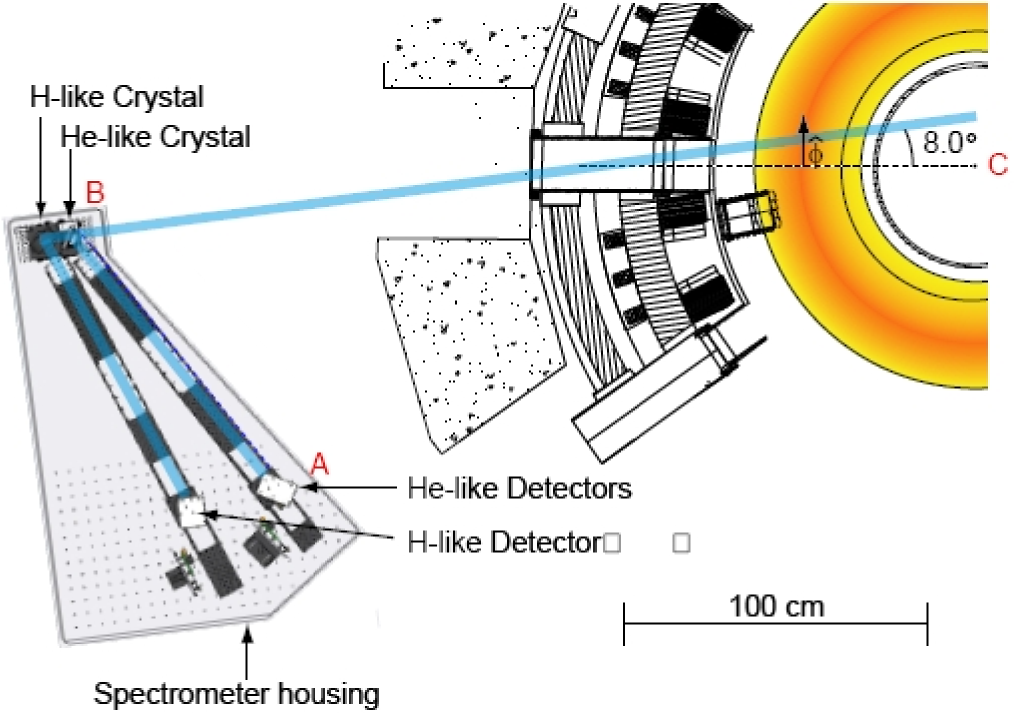

Side View

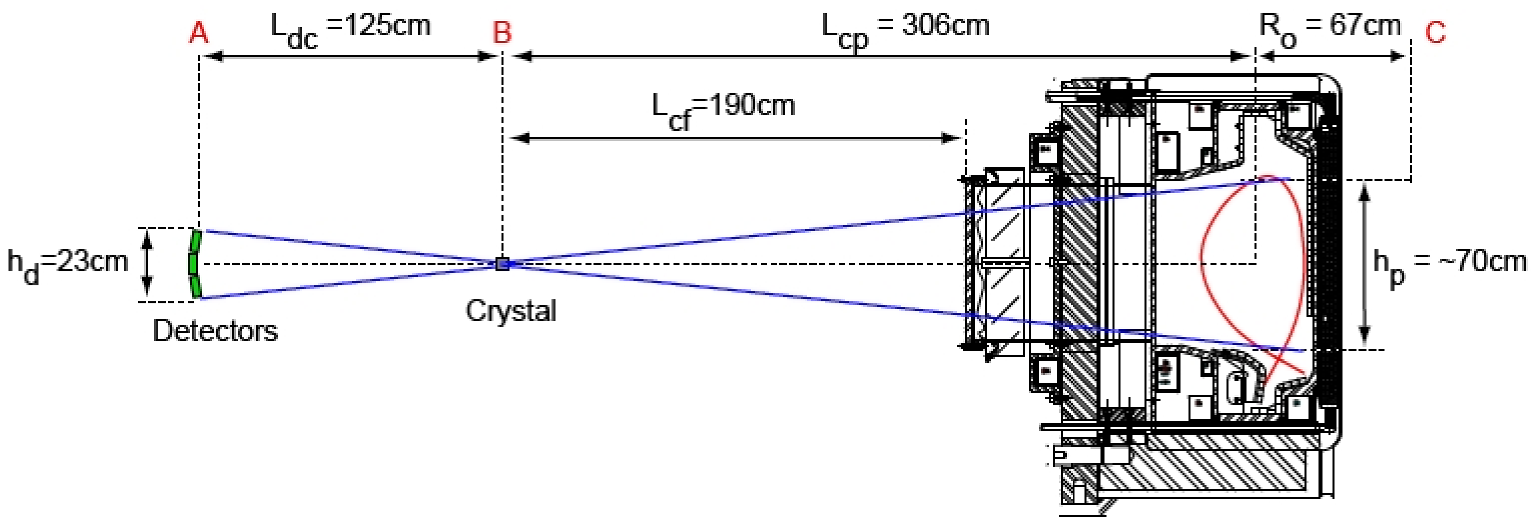

Tokamak view images to position on detectors.

Example Spatially resolved spectra

Different lines correspond to different excitations and electronic configurations.

Their relative weight is different between the plasma edge (colder) and the center (hotter).

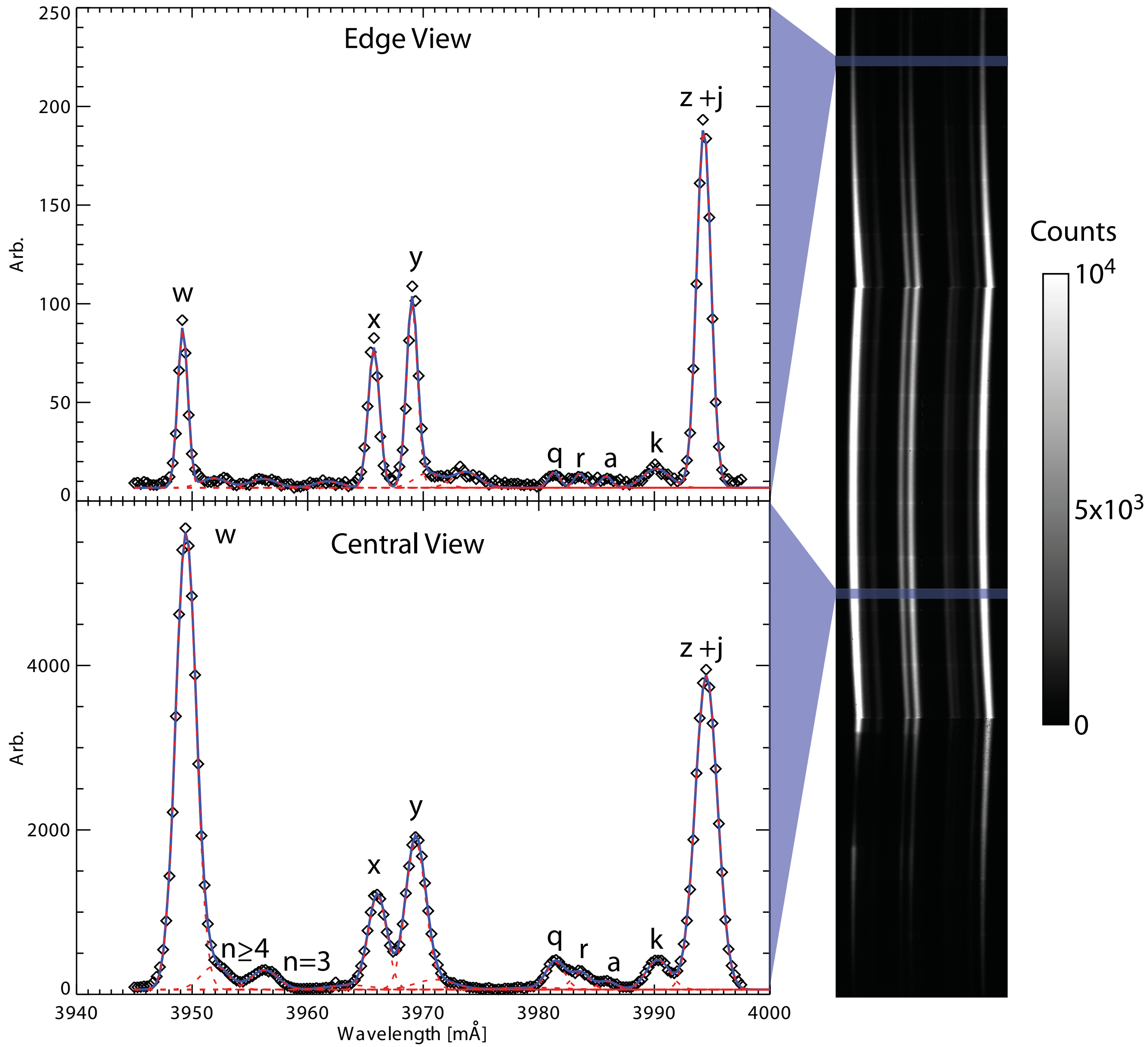

Line Width and Shift

Natural line width very small. Several broadening mechanisms arising from atom's dynamics/environment.

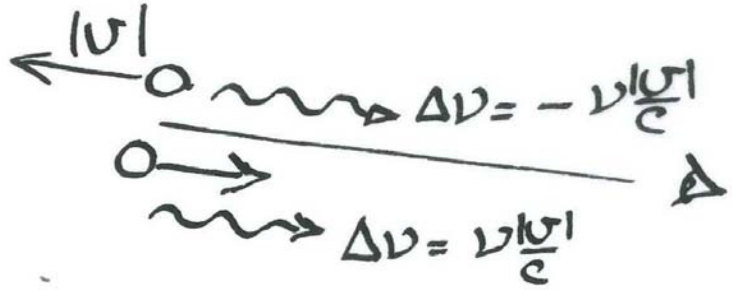

1. Doppler Shift $\quad \Delta\nu = \nu - \nu_0$

	Frequency	Wavelength	Velocity
Fractional Change	$\frac{\Delta\nu}{\nu} =$	$\left(\frac{(-)\Delta\lambda}{\lambda} \approx\right)$	$\frac{v}{c}$

Distribution of velocities: $f_i(v) \Rightarrow$ Distribution of Frequencies

Intensity as a function of frequency $\quad \boxed{I_i(\nu) \propto f\left(\frac{\Delta\nu}{\nu}\right) = f_i\left(\left[\frac{\nu}{\nu_o} - 1\right] c\right)}$

Shape of line directly reflects the atomic velocity distribution function along line of sight.

e.g. Maxwellian distribution $\quad f = \left(\frac{m_i}{2\pi T_i}\right)^{\frac{1}{2}} \exp\left(\frac{-m_i v^2}{2T_i}\right)$

leads to a Gaussian line shape: $\quad I_i(\lambda) \propto \exp\left(\frac{-m_i}{2T_i}[\frac{\lambda}{\lambda_0} - 1]^2 c^2\right)$

PSFC

Measure of Line Width

Nuclear Science & Engineering

A convenient measure of the width of a line is
Full Width Half Maximum: FWHM

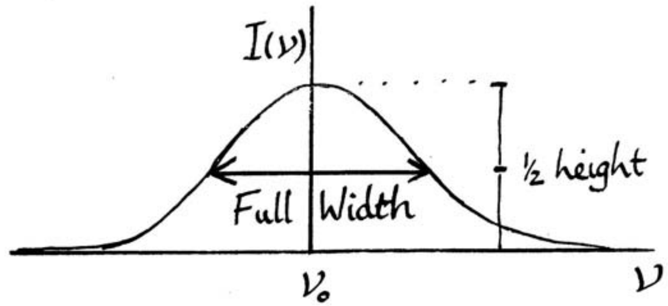

for thermal Gaussian line:

$$\boxed{\frac{\Delta\nu_{\frac{1}{2}}}{\nu_o} = \frac{\Delta\lambda_{\frac{1}{2}}}{\lambda_o} = \sqrt{2\ln 2\ \frac{T_i}{m_i c^2}}}$$

Measure **temperature** T_i from **line width** $\Delta\nu_{1/2}$.

Strictly this is *impurity species* (n_i) temperature,
but usually relaxation/equilibrium of temperatures among ions is fast so this is *ion temperature*, the same for all species: impurities, bulk ions.

Alcator C High-Resolution X-ray

$T_i \simeq 1200$eV from Doppler Broadening

Widths of Ar lines (mass 40) are visibly greater than widths of Mo lines (mass ~ 96)

because the thermal velocities are $\propto 1/m_i$. This confirms thermal.

Indicated instrumental resolution is not much smaller than line width. But can be deconvolved.

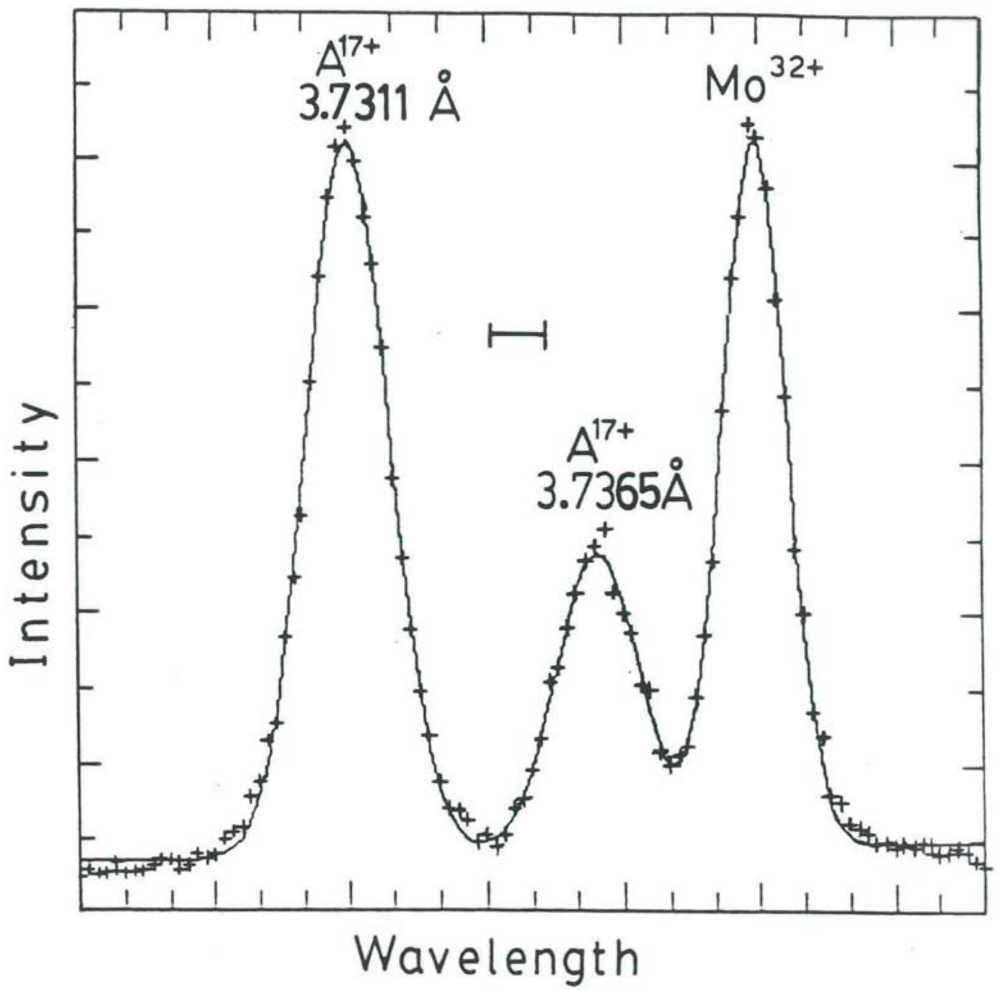

Ion Velocity Measurement

Ion flow can also be measured using line shift:

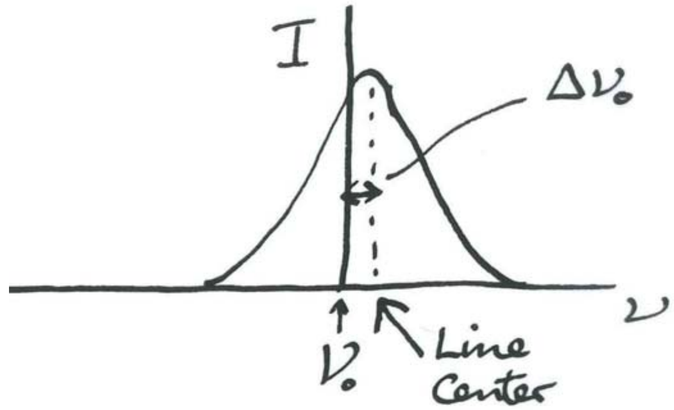

Flow velocity $V = \langle v \rangle$ is the mean over the ion/atom distribution function. Relation to line shift $\Delta\nu_o$:

$$V = \frac{\Delta\nu_o}{\nu_o} c.$$

Main limitations:

- Determine shift in presence of broadening
- Absolute wavelength determination
- Localization of sensitive volume
- Photon noise statistics.

Two Opposite Views

Helps resolve unambiguous absolute wavelength uncertainty.

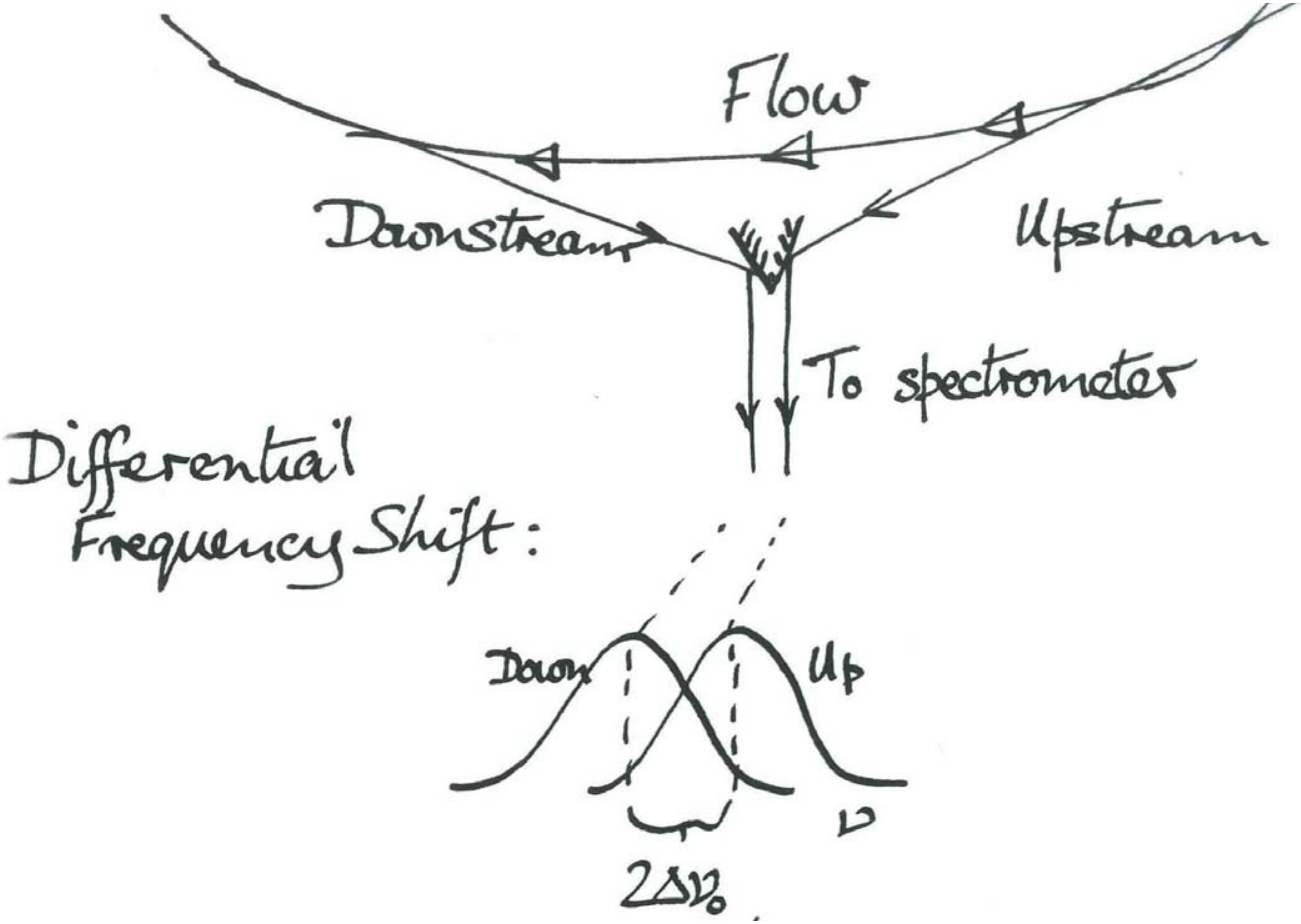

Not always available. Absolute calibration source another possibility.

Shell Structure of Ionization Stages

Different ionization stages (OI, OII, OIII, ...) exist from the coldest to the hottest regions.
So concentric "shells" of these different stages usually occur.

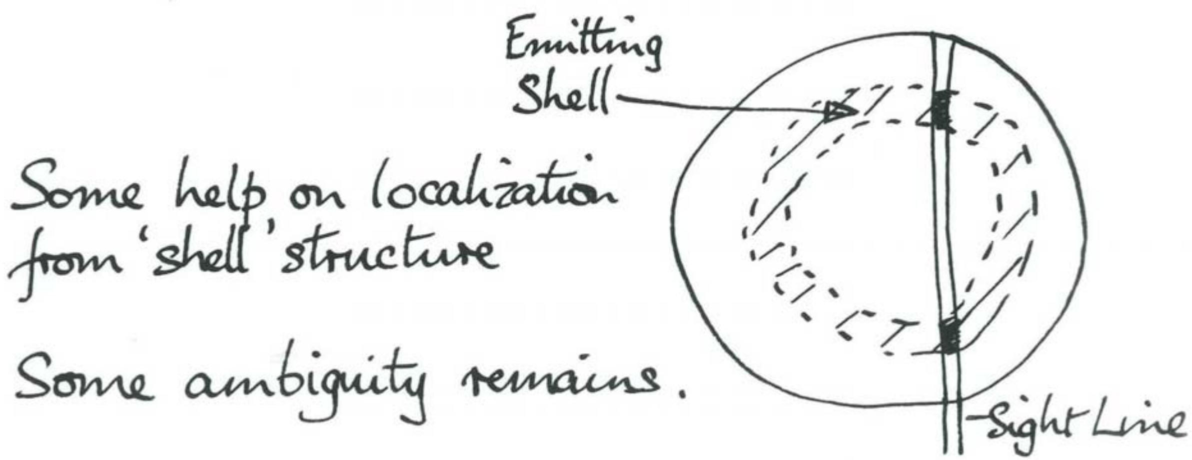

This effect gives some information about localization.
For example, the highest ionization levels occur in the center (if that's the hottest place).

However, it remains the case that the temperature and velocity measured is an *average* along the line of sight, weighted by the density of the emitting species.

We'll talk later about improvements to localization.

Stark Effect

Electric Field in which the atom resides shifts energy levels: Stark Effect.

Most atoms have polarization $\underline{p} \propto \underline{E}$ hence energy shift $\underline{p} \cdot \underline{E} \propto E^2$

quadratic shift for most atoms' lines.

However, hydrogen-like atoms have degeneracy that makes shift of energy levels larger and **linear** with the following formula for each level:

$$\underbrace{\Delta\mathcal{E}}_{\substack{\text{Energy}\\\text{Shift}}} = 3 \underbrace{n}_{\substack{\text{Principal}\\\text{Quantum No.}}} \overbrace{k}^{0,\pm1,\pm2\ldots\pm(n-1)} \underbrace{\frac{E}{Ze/4\pi\epsilon_0 a_0^2}}_{\substack{\text{Electric Field}\\\text{c.f. field at } a_0}} \underbrace{R_y}_{\substack{\text{Rydberg}\\\text{Energy}(13.6\text{eV})}}$$

[$a_0 = \hbar 4\pi\epsilon_0/e^2 m_e = 5.292 \times 10^{-11}$m, is the Bohr radius.]

Many components whose spread is proportional to E.

Both upper and lower level energy shifts must be accounted for.

Stark Broadening

Atoms reside in different E-fields arising from nearby ions.

We need the probability distribution of the E-field.

Nearest Neighbor Approximation: take E-field to be that of just the nearest neighbor $E \propto 1/r_{NN}^2$, and $\Delta\nu \propto E$.

So $I(\nu)d\nu \propto P(E)dE \propto -r_{NN}^2 dr_{NN} \propto E^{-5/2}dE$.

$$I(\nu) \propto (\Delta\nu)^{-5/2} \qquad \text{in wings}$$

Cut off of 'wings' at

$$E_0 = \frac{e}{4\pi\epsilon_0 r_0^2} \quad \text{where} \quad \frac{4}{3}\pi r_0^3 \approx \frac{1}{n_i}.$$

(Nearest can't be closer than $\sim$ this.)

Cut off at frequency shift $\Delta\nu_0$ such that

$$h\Delta\nu_0 = \Delta\varepsilon \simeq 3\frac{1}{2}n(n-1)\frac{E_0}{Ze/4\pi\epsilon_0 a_0^2}R_y$$

$$\Rightarrow \Delta\nu_0 \propto n_i^{\frac{2}{3}}$$

$$\boxed{\Delta\nu_{1/2} \propto n_i^{\frac{2}{3}}}$$

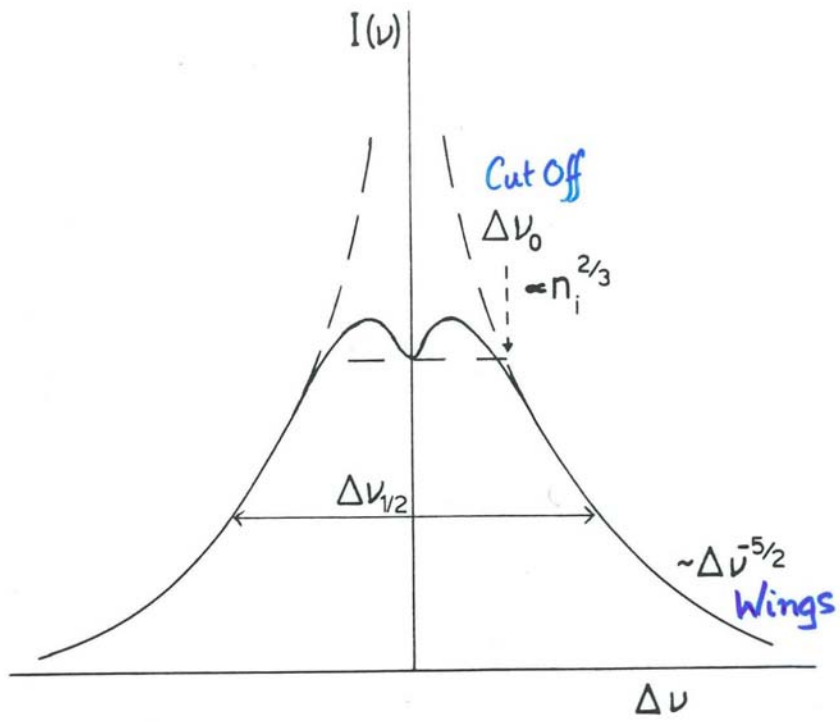

Stark Width Density Measurement

E.g. H_β:

$$\frac{\Delta\nu_{\frac{1}{2}}}{\nu_0} = \frac{\Delta\lambda_{\frac{1}{2}}}{\lambda_0} \simeq$$
$$8.2 \times 10^{-5} \left(\frac{n_e}{10^{20}m^{-3}}\right)^{\frac{2}{3}}$$

(Different coefficients other n.)

Use as a density measurement at high density, low temp$^{\underline{r}}$.

Example: detached cold, high-density divertor:

another example: pellet cloud.

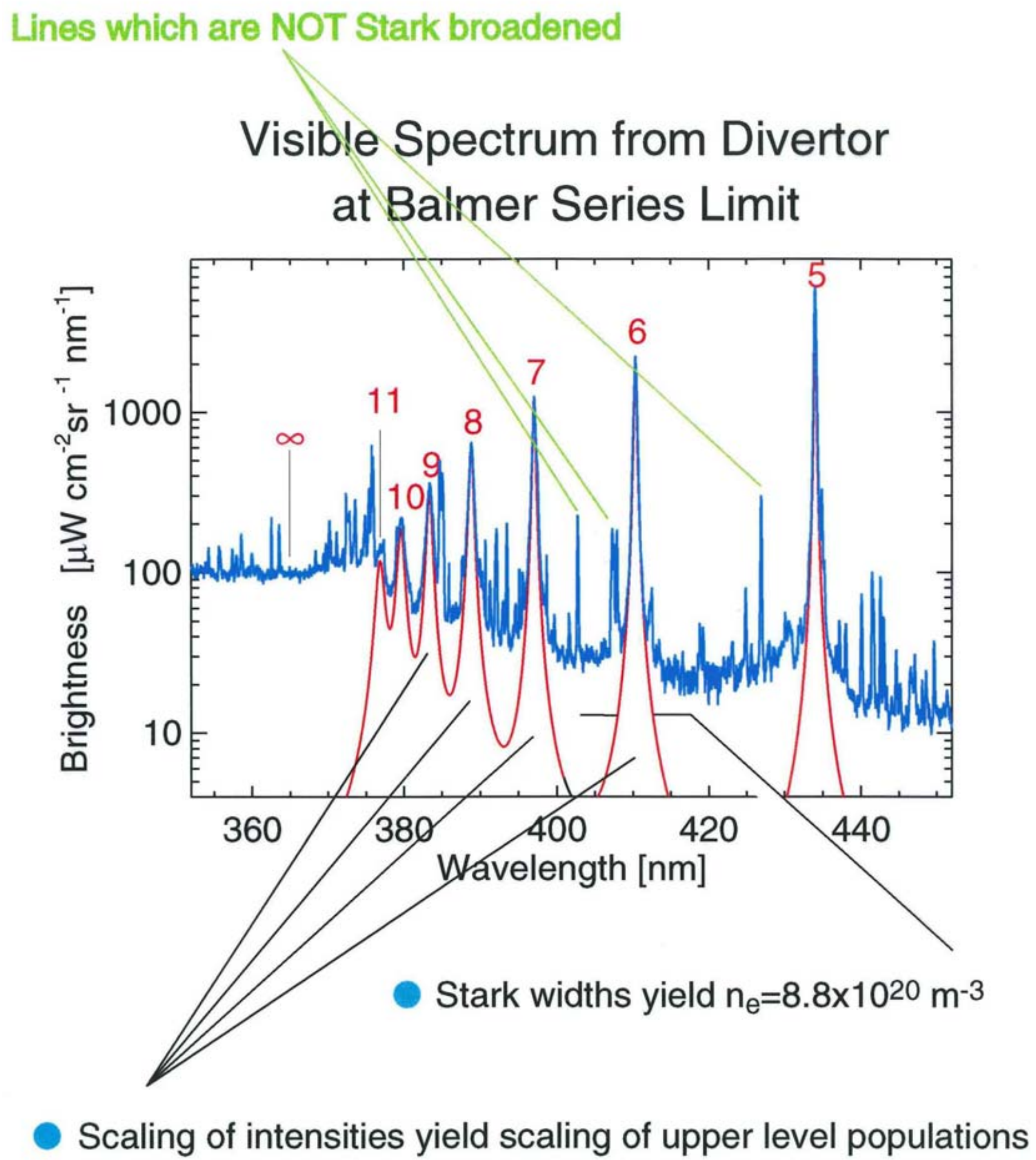

Lumma, Terry, Lipschultz, Phys Plasmas 4, 2555 (1997)

Zeeman Effect

Magnetic Field shifts energy levels by coupling to magnetic moment.

Oversimplified Line splitting

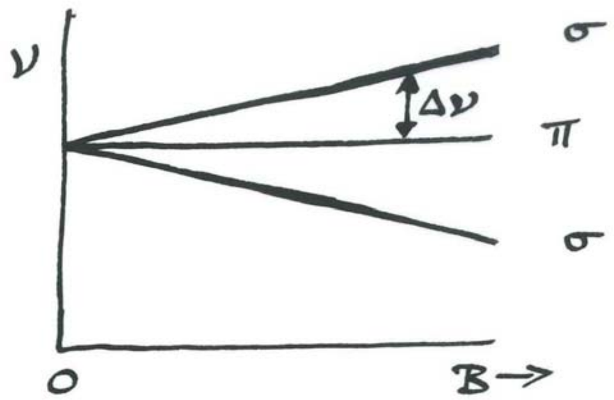

$$\boxed{\Delta\nu = \frac{1}{2\pi} g_J \, \Omega/2}$$

Landé g-factor: $g_J = 1$ orbital (~ 2 spin). Electron gyrofreqency: $\Omega = eB/m_e$

$\frac{\delta\nu}{\nu}$ is greatest for smallest ν (longest λ) hence **visible** lines (c.f. ultraviolet).

Example $B = 1T$ $\quad \Delta\nu \simeq 14$ GHz.

c.f. green light $\quad \nu \simeq 6 \times 10^5$ GHz $\quad$ giving $\dfrac{\Delta\nu}{\nu} \simeq 2.3 \times 10^{-5}$.

Compare with Doppler broadening. Doppler is bigger unless

$$T_i \lesssim (m_i c^2/2\ln 2).(2.3 \times 10^{-5})^2 \sim 1\text{eV}. \text{ (Hydrogen, } B = 1T)$$

Most hot plasma measurements are little-affected by Zeeman effect.

Zeeman Polarization

But polarization of Zeeman lines is useful: (perp. propagation)

π (unshifted) $\rightarrow$ Polarized $E_{wave} \parallel B$

σ ($\pm$ shifted) $\rightarrow$ Polarized $E_{wave} \perp B$

Measure direction of B! If different components can be separated.

To obtain visible Zeeman Effect (separable components):

Inject a monoenergetic beam of atoms (Lithium: 670.8 nm)

Beam energetic, up to 100 keV.

But energy spread, (along line of slight) can be kept small: (< 10eV)

Several successful experiments in tokamaks $\rightarrow B_p \rightarrow j_\phi^{(r)}, q^{(r)}$.

- Beam technology quite difficult
- Beam penetration limited by CX & ionization to

  $\int n_e dl \simeq 10^{18} m^{-2}$

Example Zeeman B-direction measurement

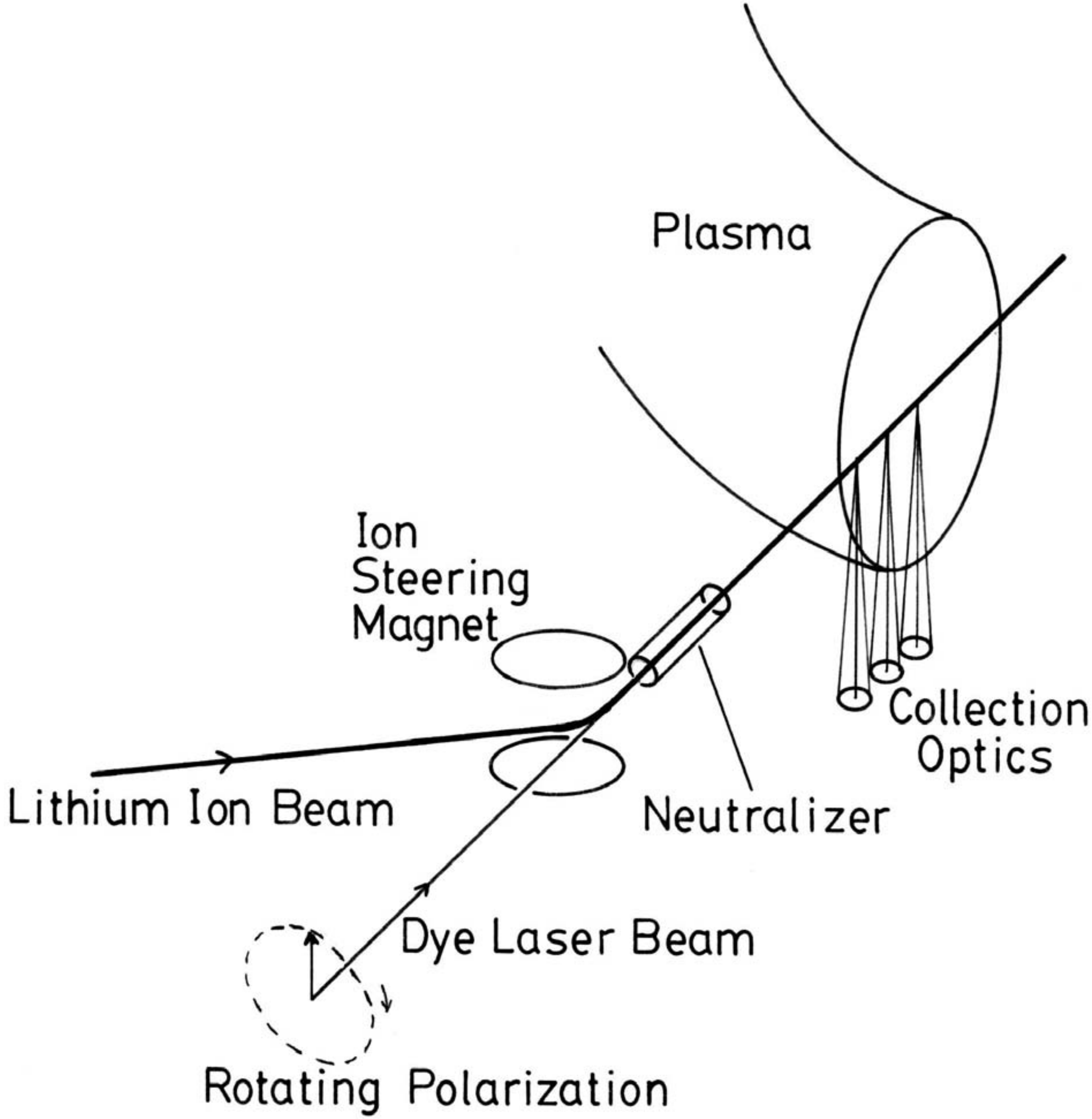

Motional Stark Effect

Particle moving in B-field experiences electric field

$$\underline{E} = \underline{v} \wedge \underline{B}$$

(Lorentz transform of EM fields).

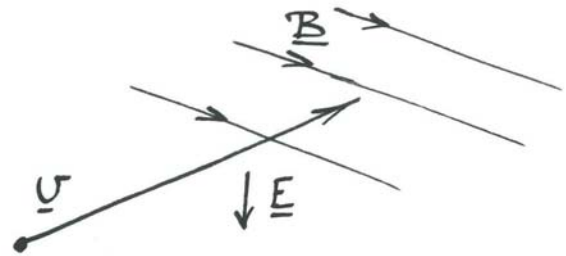

Energetic (Neutral) hydrogen beams in tokamaks experience strong E-Field.

$\longrightarrow$ Stark shifts.

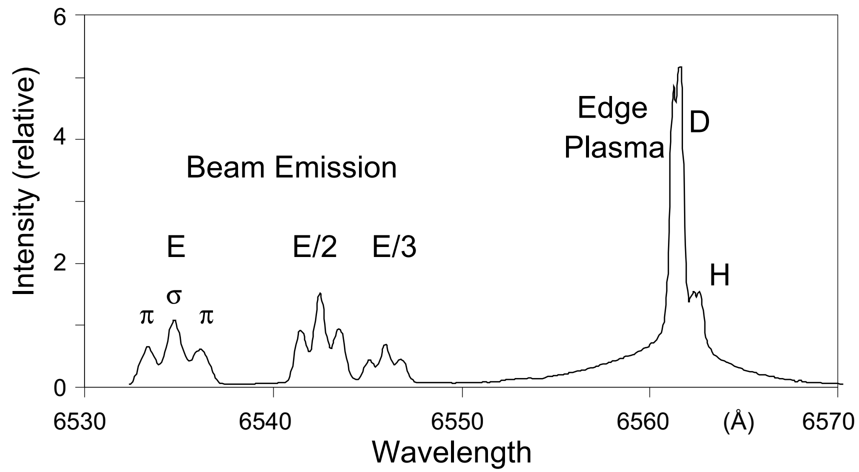

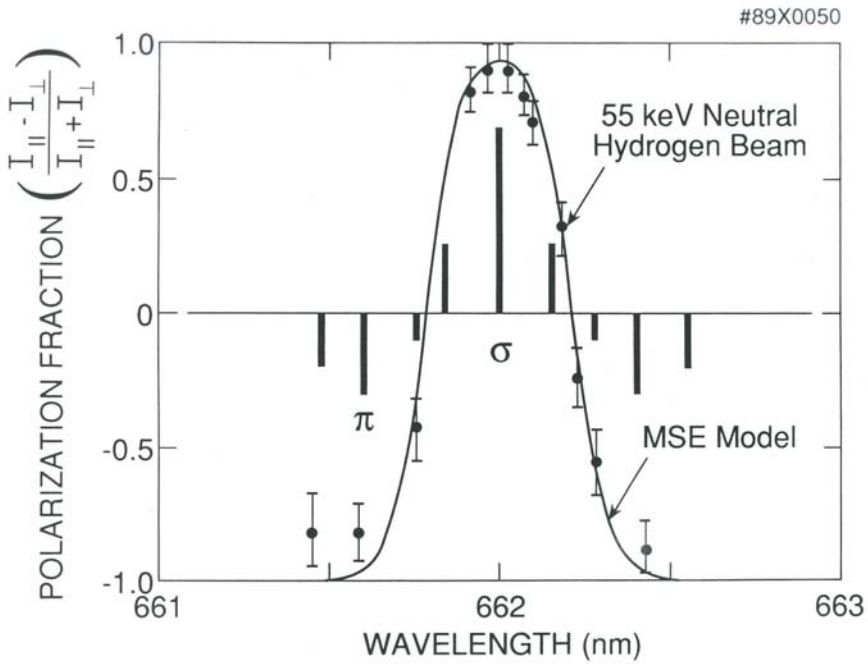

Again different Stark components have different polarizations

π $E_{\text{wave}} \parallel B$

σ $E_{\text{wave}} \perp B$.

Use to measure $\underline{B}$ direction.

F. Levinson

MSE Viewing Geometry

Earliest measurements on tokamak PBX-M

Demonstrated value of photo-elastic modulator techniques.

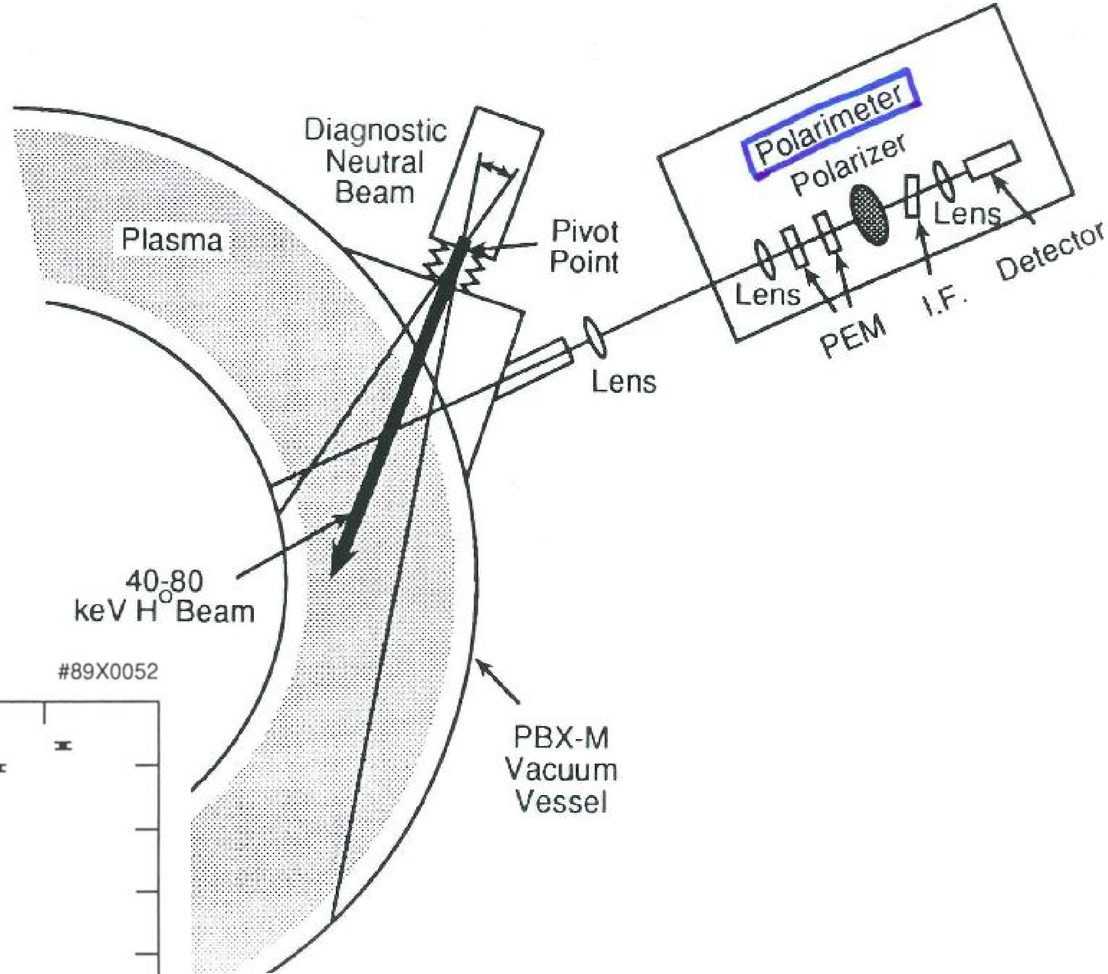

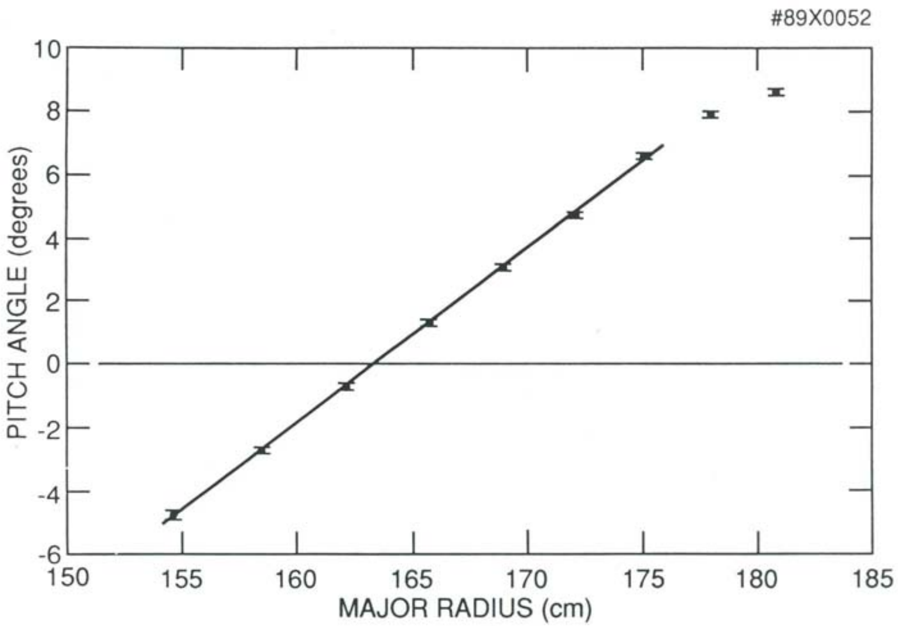

Extreme precision of polarization angle needed and obtained

Comparison with Zeeman

Advantages of Motional Stark Effect as diagnostic of B direction.

- Uses Hydrogen Beam (not e.g. Li) hence can use standard NBI heating beams and technology.
- Penetration better.
- Shift is bigger (than Zeeman) e.g., 50keV H° in 1T $\rightarrow 3.1 \times 10^6 \mathrm{Vm}^{-1}$. Then $\Delta\nu \simeq 60$ nk GHz $\sim 10\times$ Zeeman Shift.
- Well separated/polarized components
- Higher Accuracy.

Disadvantage[?]

- Sensitive to E_r.

Turn to advantage.

35 channel MSE system, using Stark polarimetry to measure both E_r and B_{pol}

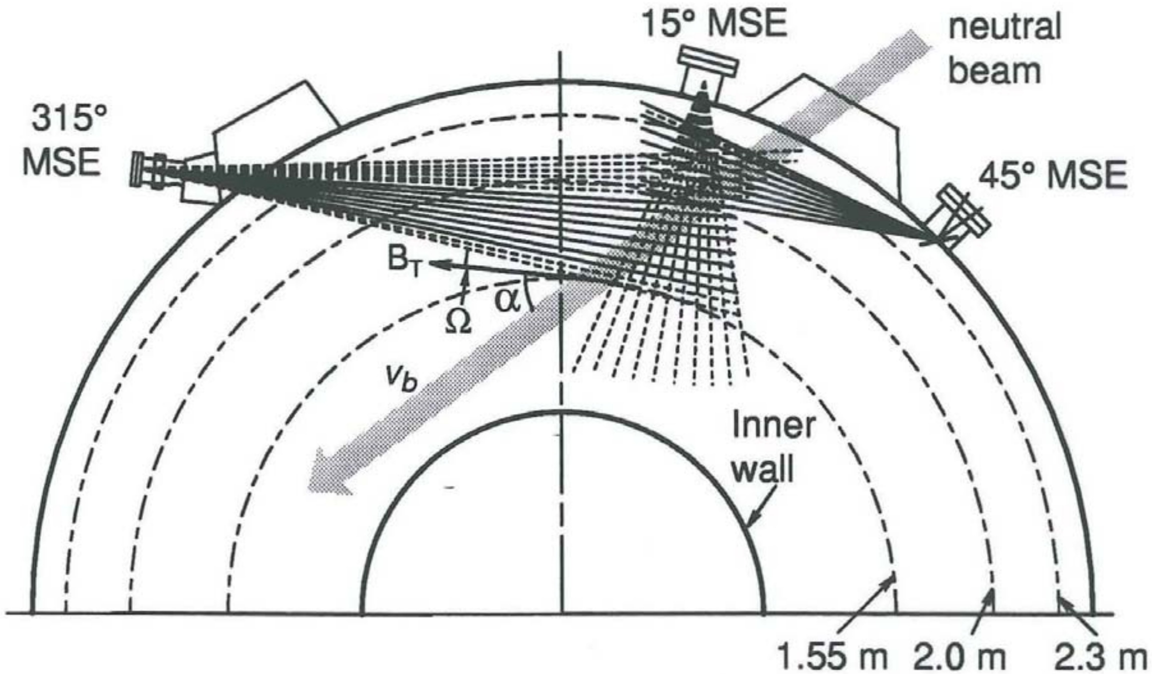

B. Rice (DIIID) 1998

Reconstruction including E_r

(a) Equilibrium reconstruction q profile obtained using all MSE chords and including E_r (solid line) versus that obtained using only tangential MSE chords and assuming $E_r = 0$ (dashed line);

(b) E_r determined from combined reconstruction with MSE data (solid line and diamonds) and determined independently from CER analysis of carbon impurities (dotted line).

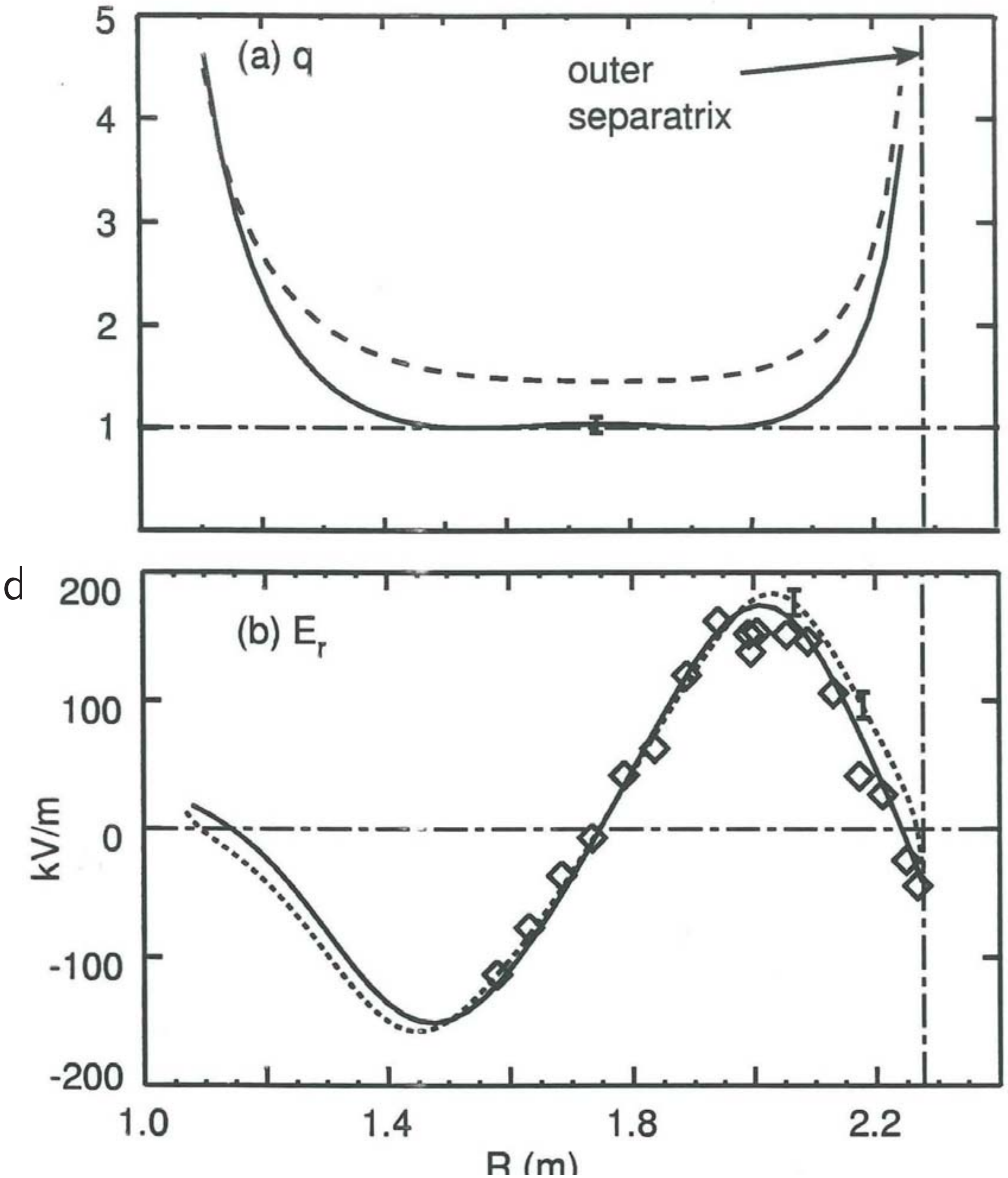

Charge Exchange Spectroscopy CXS

Nuclear Science & Engineering

Addresses three major problems with spectroscopy in high-temperature plasmas:

- Many (light) species are fully stripped. The ions have no electrons left, so they don't emit line radiation.
- Localization. We really need a way to localize the emission along collection sight-line. Crossing the view with a localized source accomplishes this.
- Visible photons that transmit through glass (or quartz) and reflect from mirrors are much easier to deal with than UV or Soft X-ray.

The Idea:

Inject an energetic beam of neutral hydrogen that intersects with the line of sight.

Charge-exchange recombination collision between beam and impurity

$$\mathrm{H}^0 + \underbrace{\mathrm{X}^{Z+}}_{\substack{\text{stripped}\\ \text{ion}}} \rightarrow \mathrm{H}^+ + \underbrace{\mathrm{X}^{*(Z-1)+}}_{\substack{\text{H-like}\\ \text{excited}}}$$

1. Creates single-electron atoms. 2. Locally to beam. 3. In excited states.

[Highly excited, and high angular momentum, states emit a cascade of lower energy (visible) photons rather than one high energy photon.]

Schematic CXS layout

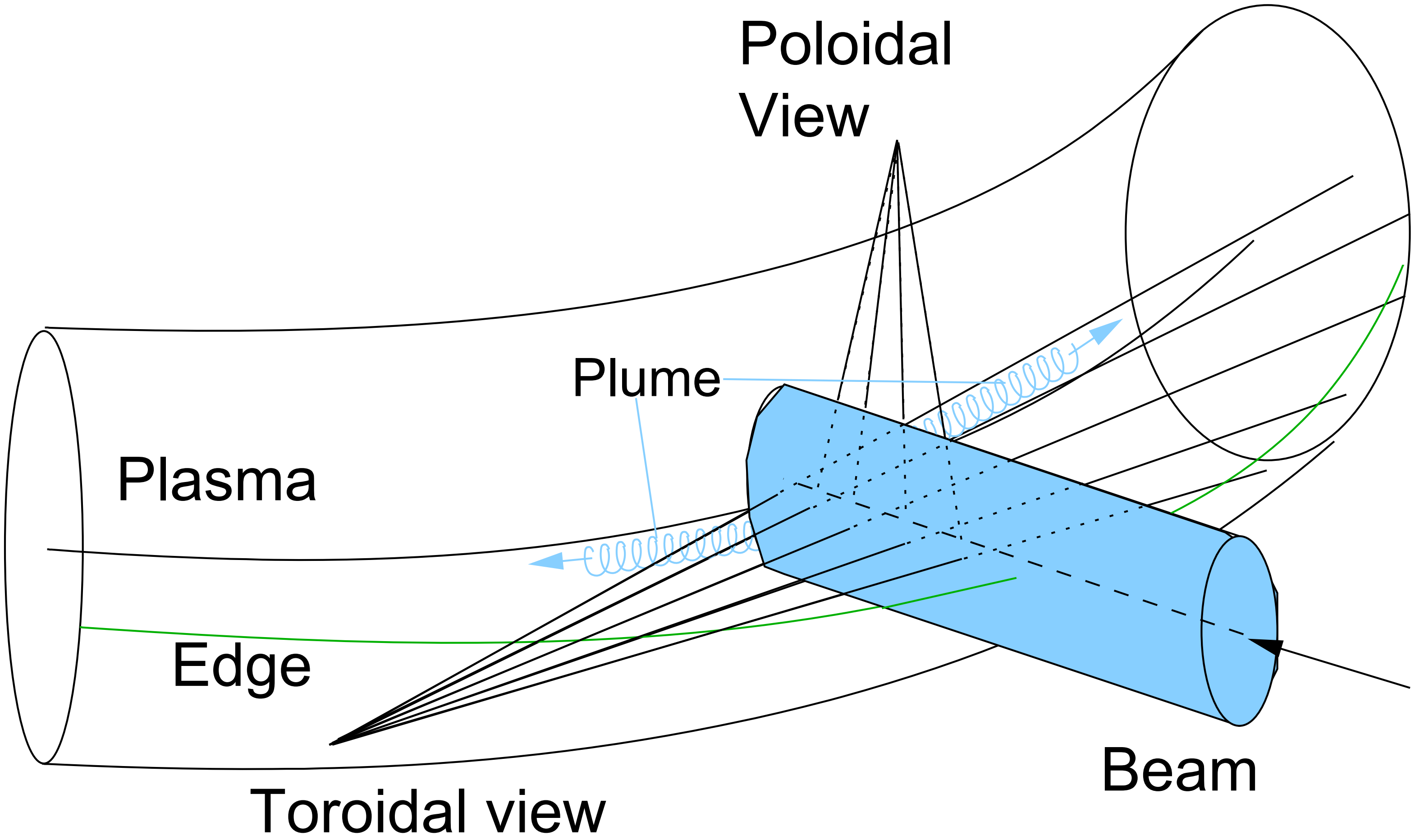

Can use the standard neutral heating beams on present experiments.

Just need appropriate views.

CX rates peak at $\sim$ 50keV/amu

Rates for production of photons by charge-exchange for various light impurities.

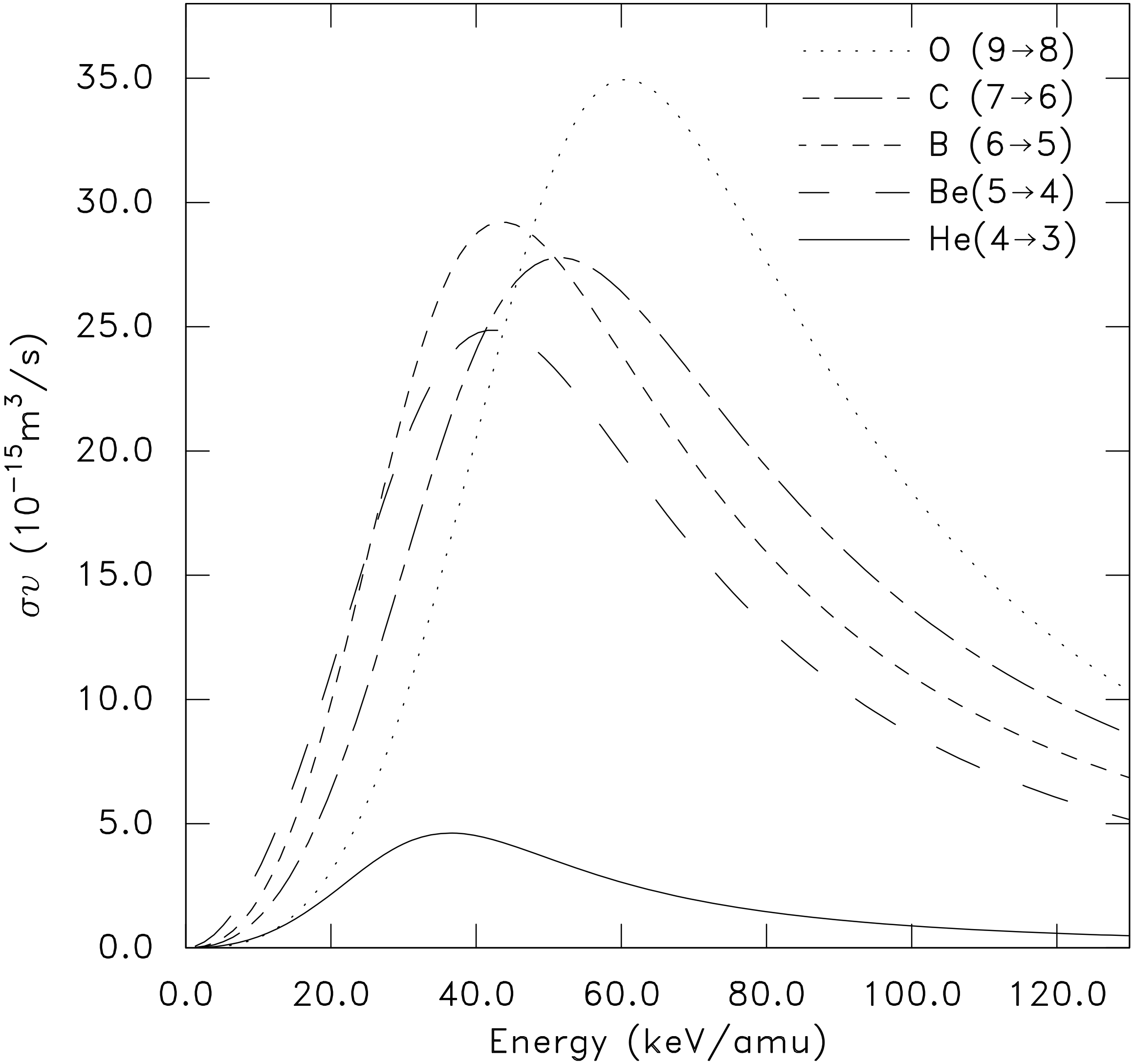

$\sim$ 50keV is also the optimal energy of positive-ion beams.

Higher energy can't be efficiently neutralized.

Lower energy does not penetrate so well.

Remarkably detailed information

Profiles of carbon: temperature, density, perpendicular and toroidal velocities,

from the edge of D-IIID tokamak.

[Courtesy K. Burrell 2001]

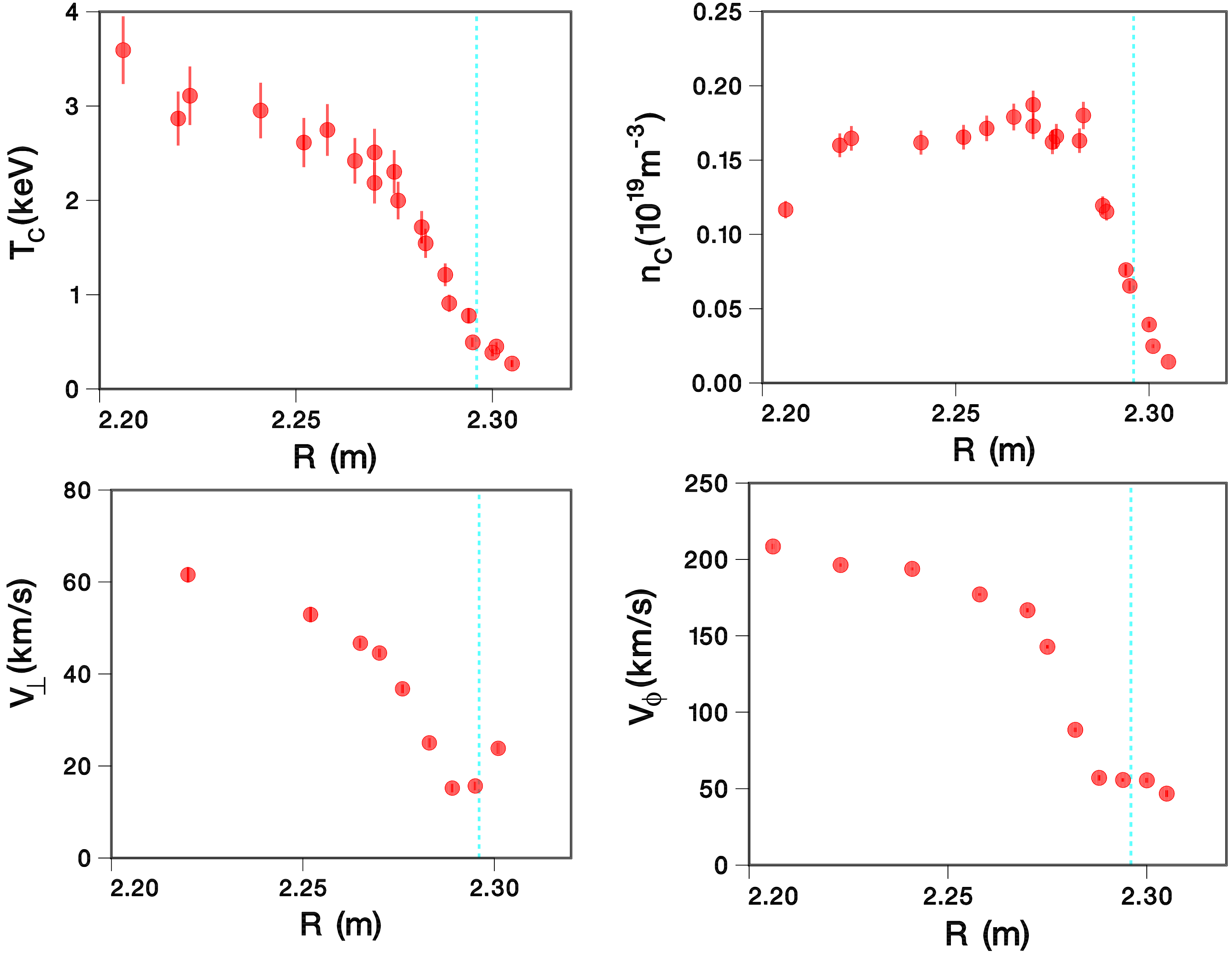

Highly influential in helping to understand the edge transport barriers.

Summary

Spectroscopic techniques give

Impurity density information from intensity.

Impurity temperature and velocity T_i, V_i from Doppler line width, shift.

Bulk density $n_e = Zn_i$ in high density, low temperature plasmas from Stark Broadening.

B-field direction from

Zeeman Effect in beams

Motional Stark Effect in beams.

Localized impurity parameters in CXS with beams.

A large fraction of all the information that we have about astrophysical plasmas.